



## City Research Online

### City, University of London Institutional Repository

---

**Citation:** Karim, M. R. & Rahman, B. M. (2016). Ultra-broadband mid-infrared supercontinuum generation using chalcogenide rib waveguide. *Optical and Quantum Electronics*, 48(3), pp. 1-10. doi: 10.1007/s11082-016-0458-5

This is the accepted version of the paper.

This version of the publication may differ from the final published version.

---

**Permanent repository link:** <https://openaccess.city.ac.uk/id/eprint/14662/>

**Link to published version:** <https://doi.org/10.1007/s11082-016-0458-5>

**Copyright:** City Research Online aims to make research outputs of City, University of London available to a wider audience. Copyright and Moral Rights remain with the author(s) and/or copyright holders. URLs from City Research Online may be freely distributed and linked to.

**Reuse:** Copies of full items can be used for personal research or study, educational, or not-for-profit purposes without prior permission or charge. Provided that the authors, title and full bibliographic details are credited, a hyperlink and/or URL is given for the original metadata page and the content is not changed in any way.

---

---

---

City Research Online:

<http://openaccess.city.ac.uk/>

[publications@city.ac.uk](mailto:publications@city.ac.uk)

---

# Ultra-broadband mid-infrared supercontinuum generation using chalcogenide rib waveguide

M. R. Karim · B. M. A. Rahman

Received: July 15, 2015 / Accepted: October 15, 2015

**Abstract** The ultrabroadband mid-infrared (MIR) supercontinuum (SC) generation using dispersion-tailored  $\text{Ge}_{11.5}\text{As}_{24}\text{Se}_{64.5}$  chalcogenide (ChG) glass rib-waveguide has been investigated numerically. An air-clad 1-cm-long rib-waveguide employing  $\text{MgF}_2$  glass for its lower cladding shows that an ultrabroadband MIR SC spanning from  $1.8 \mu\text{m}$  to  $8 \mu\text{m}$  and extending over more than 2 octave could be generated with a relatively low peak power of 0.5 kW pumped at a wavelength of  $3.1 \mu\text{m}$ . Our estimated bandwidth is the largest reported so far for SC generated using ChG rib-waveguide pumped at a wavelength of  $3.1 \mu\text{m}$  with a low peak power of 0.5 kW. We carry out simulations by varying peak power ranges between 0.1 kW and 3 kW. Our analysis through rigorous numerical simulations show that SC can be extended further into the MIR up to  $10 \mu\text{m}$  using the same pump pulses with a relatively modest peak power of 3 kW.

**Keywords** Numerical approximation and analysis · Nonlinear optics · Glass waveguides · Supercontinuum generation

## 1 Introduction

Supercontinuum (SC) generation using nonlinear effects in optical waveguides attracted a lot in nonlinear optics as its use provides an optical source with properties such as large bandwidth, brightness, high coherence, and potential compactness (Andreasen et al. 2014; Dudley et al. 2006). The generation of ultra-broadband SC spectra from ultraviolet to mid-infrared (MIR) region is of considerable interest for many applications in the field of telecommunication, molecular fingerprint spectroscopy, bio-imaging, pulse compression, optical coherence tomography, high

---

M. R. Karim

School of Mathematics, Computer Science and Engineering, City University London, Northampton Square, London, EC1V 0HB, UK

E-mail: mohammad.karim.2@city.ac.uk

B. M. A. Rahman

School of Mathematics, Computer Science and Engineering, City University London, Northampton Square, London, EC1V 0HB, UK

precision frequency metrology, and optical sensing (Dudley et al. 2009; Eggleton et al. 2011; Shaw et al. 2011). There is a strong motivation to fabricate SC sources operating in the molecular fingerprint region of the optical spectrum in the range 2-20  $\mu\text{m}$  both for sensing illicit or dangerous materials via their spectroscopic signatures and for applications such as MIR astronomy (Petersen et al. 2014; Wei et al. 2013). Although SC generation inside optical fibers has been used to produce broadband spectra that cover the visible and near-infrared regions, silica fibers cannot be used in the MIR region of their high losses in that spectral range. Moreover, the intrinsic transmission window of fused silica makes SC expansion beyond 2.2  $\mu\text{m}$  a challenging task which caused a gradual shift towards other types of glasses such as ZBLAN and tellurite fibers which have higher transparency in the long wavelength region. However, the propagation losses of such fibers become intolerably large in the long wavelength region (Fatome et al. 2009; Hu et al. 2010; Weiblen et al. 2010). In recent years chalcogenide (ChG) glasses are emerging as promising nonlinear materials in the MIR region transparency extending from 1 to 20  $\mu\text{m}$  (Aggarwal et al. 2002). Such glasses have a number of unique properties which make them attractive for fabricating optical planar waveguides, including low nonlinear absorption, low TPA, no FCA, and fast response time because of the absence of free-carrier effects. Moreover, ChG glasses exhibit high optical Kerr nonlinearities which is several hundred times larger than that of silica (Gai et al. 2010; Lamont et al. 2007). Therefore, researches have focussed recently in most theoretical and experimental investigation on chalcogenide based planar waveguides (Gai et al. 2012; Lamont et al. 2008; Ma et al. 2013; Yu et al. 2013; Yu et al. 2014) and step-index fibers (Hudson et al. 2014; Kubat et al. 2014; Møller et al. 2015; Petersen et al. 2014; Shaw et al. 2011; Yu et al. 2015) for extending SC further into the MIR regime.

We have shown in this paper numerically that a 1-cm-long, dispersion-tailored,  $\text{Ge}_{11.5}\text{As}_{24}\text{Se}_{64.5}$  ChG air-clad rib waveguide employing  $\text{MgF}_2$  glass as its lower cladding can be used to generate a ultra-broadband SC in the MIR region. Several research groups have shown experimentally that the extension of SC in the long wavelength region depends on the availability of pump pulses at a suitable wavelength. In particular, the pump wavelength needs to be near 3-4  $\mu\text{m}$  or longer (Møller et al. 2015; Yu et al. 2014). To tailor the dispersion around this pump wavelength, the effective mode area of the waveguide is often increased which, in turn, decreases the nonlinear parameter of the waveguide. As the nonlinear coefficient of a ChG waveguide also decreases with the increasing pump wavelength, high pump powers are required to extend SC in the MIR region, which can cause damage to ChG waveguides if relatively wide pump pulses with high peak powers are employed (Yu et al. 2013). For our numerical simulations, we employ pump pulses of 85 fs duration (FWHM) at a wavelength of 3.1  $\mu\text{m}$  with a repetition rate of 160 kHz (Silva et al. 2012). The peak power of pump pulses is varied in the range of 0.1 to 3 kW. It is numerically found that the SC can be extended over more than 2 octave covering the wavelength range of 1.8-8  $\mu\text{m}$  (at the  $-30$  dB level from the peak) with relatively low peak power of 0.5 kW. The SC covering the wavelength range from 1.8 to 10  $\mu\text{m}$  can be generated with our proposed ChG rib waveguide at a relatively moderate peak power of 3 kW.

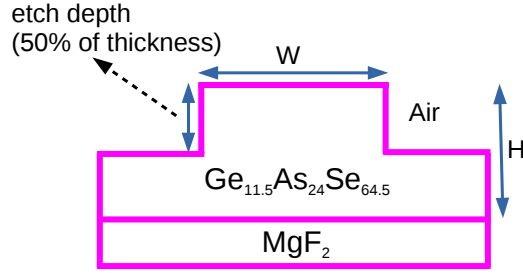


**Fig. 1** ChG rib-waveguide structure used for group velocity dispersion (GVD) optimization.

## 2 Theory

The schematic diagram of the  $\text{Ge}_{11.5}\text{As}_{24}\text{Se}_{64.5}$  ChG glass rib waveguide used in our simulations is shown in Fig. 1. The wavelength-dependent linear refractive index of  $\text{Ge}_{11.5}\text{As}_{24}\text{Se}_{64.5}$  and  $\text{MgF}_2$  glasses over the entire wavelength range used in the simulation was obtained using the following Sellmeier equation,

$$n^2(\lambda) = 1 + \sum_{i=1}^m \frac{A_i \lambda^2}{\lambda^2 - \lambda_i^2}, \quad (1)$$

Here  $\lambda$  is the wavelength in micrometers. We use the Sellmeier coefficients calculated by fitting smooth curves to the measured refractive index data for the  $\text{Ge}_{11.5}\text{As}_{24}\text{Se}_{64.5}$  (Ma et al. 2013) and the  $\text{MgF}_2$  (Bass et al. 2010) glasses. The values of the integer  $m$  and the fitting coefficients are given in Table 1.

**Table 1** Sellmeier fitting coefficients

Material	$\text{Ge}_{11.5}\text{As}_{24}\text{Se}_{64.5}$		$\text{MgF}_2$	
	1		2	
$m$	$A_i$	$\lambda_i$	$A_i$	$\lambda_i$
$i = 1$	5.78525	0.287950	0.48755708	0.04338400
$i = 2$	0.39705	30.39338	0.39875031	0.09461442
$i = 3$	-	-	2.31203530	23.7936040

SC is a complex spectral broadening generated at the output of the optical waveguide which involves the interplay between linear and nonlinear phenomena that occur during the propagation of the optical signal inside the waveguide. Dispersion which is a linear effect interacting with nonlinearity of the waveguide plays an important role in producing the broadband SC in the ChG waveguide output. A relatively small anomalous dispersion over a wide wavelength range is required for large frequency shifts of the Raman soliton forming inside the waveguide. ChG glasses generally have smaller material dispersion than silicon. To realize waveguide's zero-dispersion wavelength (ZDW) close to the pump wavelength, relatively larger waveguide dispersion is required to offset the material dispersion. To obtain dispersion coefficient for our proposed ChG waveguide at a pump wavelength,

we use a FE based full-vectorial mode-solver (Rahman et al. 1984) to obtain the propagation constant of the fundamental quasi-TE mode over a wide range of wavelengths. To calculate the effective mode index, which is used for calculating various higher-order dispersion parameters, we utilize the mode propagation constant obtained through our FE mode-solver.

The FE method is a well established numerical method for the solution of a wide range of guided-wave problems. It can be easily applied to optical waveguides with any refractive index distribution and to those with anisotropic or nonlinear materials. The FE method is based upon dividing the waveguide region into a large number of non-overlapping triangular elements. The field over each element is then expressed in terms of polynomials weighted by the fields over each element. By differentiating the functional with respect to each nodal value, the problem is reduced to a standard eigenvalue matrix equation, which is solved to obtain the propagation constants  $\beta(\omega)$  and field profiles of various modes. In the full-vectorial formulation one needs to minimize the full  $\mathbf{H}$ -field energy functional using (Rahman et al. 1984),

$$\omega^2 = \frac{\iint_{\Omega} [(\nabla \times \mathbf{H})^* \cdot \hat{\epsilon}^{-1} (\nabla \times \mathbf{H}) + p(\nabla \cdot \mathbf{H})^* (\nabla \cdot \mathbf{H})] d\Omega}{\iint_{\Omega} \mathbf{H}^* \cdot \hat{\mu} \mathbf{H} d\Omega}, \quad (2)$$

where  $\mathbf{H}$  is the vectorial magnetic field,  $*$  denotes a complex conjugate and transpose,  $\omega$  is the angular frequency,  $p$  is a weighting factor for the penalty term to eliminate spurious modes,  $\Omega$  is the computational domain, and  $\hat{\epsilon}$  and  $\hat{\mu}$  are the permittivity and permeability tensors, respectively.

The process of SC generation can be studied in our proposed rib waveguide by solving generalized nonlinear Schrödinger equation (GNLSE). For modeling SC generation inside the waveguide, it is important to include the dispersion parameters and intrapulse Raman scattering into GNLSE as accurately as possible. Therefore, we model the pulse evolution inside our proposed waveguide using GNLSE from Gai et al. (2010):

$$\begin{aligned} \frac{\partial}{\partial z} A(z, T) = & -\frac{\alpha}{2} A + \sum_{m \geq 2} \frac{i^{m+1}}{m!} \beta_m \frac{\partial^m A}{\partial T^m} + i \left( \gamma + i \frac{\alpha_2}{2A_{\text{eff}}} \right) \left( 1 + \frac{i}{\omega_0} \frac{\partial}{\partial T} \right) \\ & \times \left( A(z, T) \int_{-\infty}^{\infty} R(T') |A(z, T - T')|^2 dT' \right), \quad (3) \end{aligned}$$

where  $A(z, T)$  is the slowly varying envelope of the pump pulse in a retarded time frame  $T = t - \beta_1 z$  moving at the group velocity  $1/\beta_1$ ,  $\beta_m$  ( $m \geq 2$ ) is the  $m$ th order dispersion parameter,  $\alpha$  accounts for linear propagation losses, and  $\omega_0$  is the pump angular frequency. The nonlinear coefficient is defined as  $\gamma = n_2 \omega_0 / (c A_{\text{eff}})$ , where  $n_2$  is the nonlinear refractive index,  $c$  is the speed of light in vacuum,  $A_{\text{eff}}$  is the effective area of the mode at the pump frequency, and  $\alpha_2 = 9.3 \times 10^{-14}$  m/W is the two-photon absorption coefficient (Gai et al. 2010). The material response function  $R(t)$  includes both the instantaneous Kerr response,  $\delta(t)$ , and the delayed Raman response,  $h_R(t)$ , expressed as

$$R(t) = (1 - f_R) \delta(t) + f_R h_R(t), \quad (4)$$

$$h_R(t) = \frac{\tau_1^2 + \tau_2^2}{\tau_1 \tau_2} \exp\left(-\frac{t}{\tau_2}\right) \sin\left(\frac{t}{\tau_1}\right). \quad (5)$$

where  $f_R = 0.031$ ,  $\tau_1 = 15.5$  fs, and  $\tau_2 = 230.5$  fs for ChG material (Granzow et al. 2011).

### 3 Dispersion tailoring of a ChG rib-waveguide

Since the MIR SC generation requires the cladding as well as core materials of a waveguide to be transparent at long wavelengths, we designed and optimized a rib waveguide made using air as upper cladding and  $\text{MgF}_2$  glass as lower cladding, whose refractive index of 1.33 at  $3.1 \mu\text{m}$  provides an index contrast of 1.3. By varying waveguide dimensions for realizing ZDW around the pump wavelength, we numerically calculated GVD for this structure as a function of wavelength for the fundamental quasi-TE mode and plot it with material dispersion in Fig. 2. It can be observed from this figure that the material dispersion, shown by a dashed black line, remains normal for the wavelength range  $1.5 \mu\text{m}$  to  $5.5 \mu\text{m}$ , considered here but the total dispersion curve, shown by a solid red line, reached to the anomalous dispersion region between the  $2.5 \mu\text{m}$  (1st ZDW) and  $4.8 \mu\text{m}$  (2nd ZDW) due to tailoring dispersion through the variation of transverse dimensions of the rib waveguide. The GVD value estimated at the pump wavelength is around  $32 \text{ ps/nm/km}$ . Due to asymmetric waveguide structure, this waveguide geometry supports propagation of the fundamental quasi-TE mode up to the cut-off wavelength beyond  $12 \mu\text{m}$ .

The design of an optical waveguide for SC generation depends on GVD and higher-order dispersion parameters. The accuracy of dispersion parameters depend on how accurately calculates the mode propagation,  $\beta(\omega)$  for the fundamental mode through FE modal solutions. Therefore, accuracy of any design critically de-

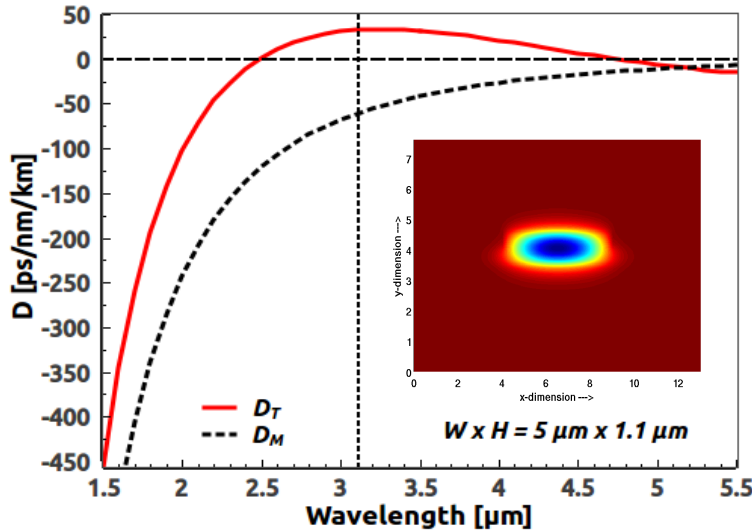


**Fig. 2** GVD curve (solid red line) tailored for the fundamental quasi-TE mode calculated from effective index ( $n_{\text{eff}}$ ) and dashed black line curve represents the material dispersion ( $D_M$ ) of  $\text{Ge}_{11.5}\text{As}_{24}\text{Se}_{64.5}$  ChG material. Vertical dotted line indicates pump wavelength and the inset shows the spatial profile of the fundamental mode at a wavelength of  $3.1 \mu\text{m}$ .

depends on the accuracy of modal solutions of a waveguide. For our rib-waveguide, we represent the waveguide structure with 360,000 first order triangular elements across the transverse dimensions to obtain higher accuracy modal solutions. A powerful extrapolation technique (Rahman et al. 1985) was used to test the accuracy of modal solution for this waveguide structure. We tested the FE results by Aitken's extrapolation through convergence between the raw FEM results and extrapolated values as the number of elements increased. Using the FE method described above we have obtained modal solutions from which mode propagation constant  $\beta(\omega)$  of the fundamental mode over a range of frequencies are evaluated and calculate the effective index ( $n_{\text{eff}} = \lambda\beta(\omega)/2\pi$ ) from the mode propagation constant obtained through modal solutions. We also tested the GVD curves obtained through FE mode-solver by the data fitting method applying Taylor series expansion. It was observed good matching between the two which made us confident about the GVD curve obtained through FE mode-solver.

Inset of Fig. 2 shows the field profile of the fundamental quasi-TE mode of the ChG rib waveguide at a pump wavelength of  $3.1 \mu\text{m}$  for the waveguide geometry,  $W = 5 \mu\text{m}$  and  $H = 1.1 \mu\text{m}$  employing air as upper and  $\text{MgF}_2$  glass for its lower claddings. It is apparent from the figure that the field representation inside the core as well as along the transverse dimensions of the structures that the mode is highly confined inside the rib waveguide owing to using large index contrast cladding material. As the mode field is highly confined along the thickness due to using larger index contrast material for its lower cladding resulting in lower  $A_{\text{eff}}$  which, in turn, increases nonlinearity of the waveguide. The spatial profile of the fundamental mode, shown as an inset of Fig. 2, exhibits excellent field confinement to the central core region which thus enables an enhanced nonlinear interaction.

#### 4 SC generation in a ChG rib-waveguide

For demonstrating SC generation, the generalized nonlinear Schrödinger equation were solved numerically using split-step Fourier method. Our previous study shows that there is a possibility to obtain spurious results if the inadequate number of higher-order dispersion coefficients is included during numerical simulations for SC generation (Karim et al. 2014). So, we calculate, from GVD curve, higher-order dispersion terms up to  $10^{\text{th}}$  order for adding in SC simulations. The temporal grid length must be wide enough consisting of a number of smaller time-steps so that it can accommodate extreme spectral broadening during pulse propagation containing maximum frequency of the field. Therefore, a small time-step was chosen which was sufficient for capturing the broadband SC spectrum generated after the numerical simulations. As the GeAsSe-based glass has the lowest damage threshold at an average power density of  $30 \text{ kW/cm}^2$ , paying attention to this factor, we designed our rib waveguide for MIR SC generation such that the required peak power of pump pulses is at most 3 kW. The linear propagation loss of ChG waveguides due to material absorption is almost negligible in short waveguides design. Although we proposed 1-cm-long rib waveguide, the linear propagation loss ( $\alpha$ ) at a pump wavelength of  $3.1 \mu\text{m}$  we consider here is  $0.5 \text{ dB/cm}$  (Ma et al. 2013). The value of nonlinear refractive index used in our simulations was reduced by a factor of two from its known value of  $n_2 = 5.2 \times 10^{-18} \text{ m}^2/\text{W}$  at  $1.55 \mu\text{m}$  (Yu et al. 2014). The effective mode area was calculated numerically by using our FE

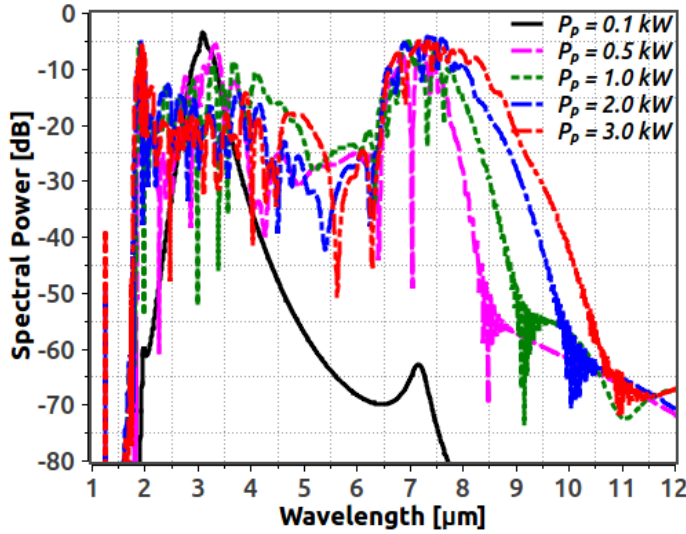


**Fig. 3** Simulated SC spectra at a pump wavelength of  $3.1 \mu\text{m}$  for rib waveguide with peak power varies between 0.1 kW and 3 kW.

mode-solver which is  $A_{\text{eff}} = 3.86 \mu\text{m}^2$ , yielding a nonlinear coefficient of  $\gamma = 2.26 \text{ W}^{-1}/\text{m}$  at the pump wavelength of  $3.1 \mu\text{m}$ .

To predict SC generation in our proposed waveguide, we have carried out numerical simulations using Eq. (3) launching a TE polarized 85-fs FWHM secant pulse pumped at a wavelength of  $3.1 \mu\text{m}$  for peak power levels between 0.1 and 3 kW and the results are shown in Fig. 3. The SC spectrum extends farther into the long-wavelength region with increasing pump power as expected. For the largest peak power of 3 kW, SC extended up to  $10 \mu\text{m}$  at a spectral power level of  $-30 \text{ dB}$  from the peak. However, SC extended more than two octave covering the wavelength range  $1.8\text{--}8 \mu\text{m}$  for relatively low peak power of 0.5 kW.

The dynamics of SC generation is well-known. However, we will here make a numerical investigation of the SC generation as well as explain the influence of Raman contribution in the spectral broadening process. The spectra shown in Fig. 3 does not reveal how the SC evolves inside the waveguide. Figures 4(b)-4(d), 5(b)-5(d) demonstrate the temporal evolution, spectral evolution and spectrogram of pump pulses along the 1-cm length of the waveguide for the peak power levels of 0.5 kW and 3 kW, respectively. The dispersion lengths of the 85-fs pump pulse in these power level is  $L_D = 14.1 \text{ mm}$  and the corresponding nonlinear lengths at a peak power of 0.5 and 3 kW are  $L_{\text{NL}} = 0.15$  and  $0.89 \text{ mm}$ , respectively. These values correspond to soliton orders  $N = \sqrt{L_D/L_{\text{NL}}}$  of about 4 and 10 for the peak power levels 0.5 and 3 kW, respectively. In both cases, SC formation is mainly dominated by the soliton fission process occurring at a distance of 3.5 mm and 1.4 mm observed in Figs. 4(b)-4(c) and 5(b)-5(c), respectively. As the pump lies in the anomalous GVD regime, SC generation is mainly dominated by the soliton fission process. Soliton fission occurs at a distance of soliton fission length for both cases mainly because of perturbation induced by third and higher-order dispersions. Due to the perturbation induced by the third and all odd-order disper-

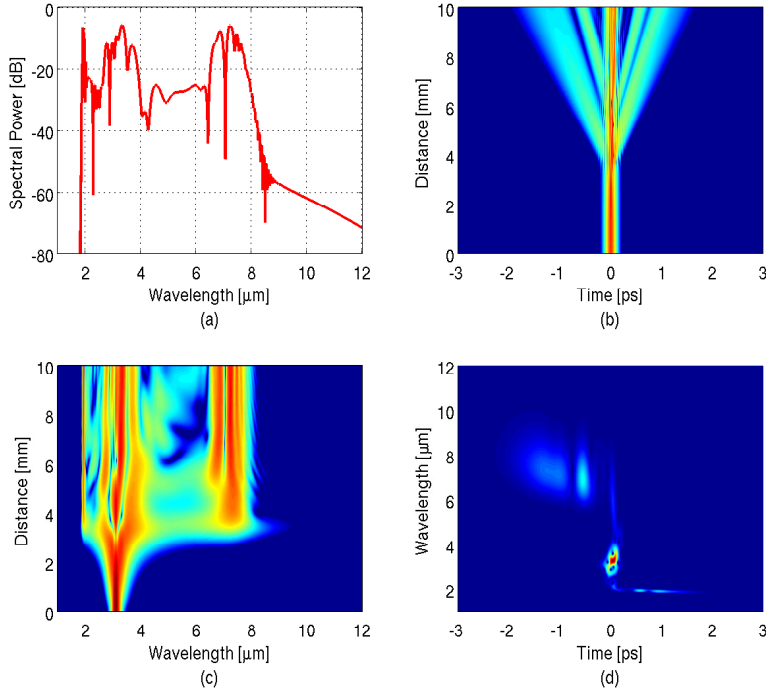


**Fig. 4** Spectral evolution along the waveguide length at a wavelength of  $3.1 \mu\text{m}$  for the peak power of  $0.5 \text{ kW}$ : (a) spectrum; (b) temporal density; (c) spectral density; and (d) spectrogram.

sion coefficients, multiple fundamental solitons are produced according to soliton order after the fissions, whose spectra shift toward the longer wavelength sides (stoke-side) because of Raman induced frequency shift (RIFS), producing multiple spectral peaks in the spectrum. One can also observe that a dispersive wave is generated at a wavelength near the first ZDW (located at around  $2.5 \mu\text{m}$ ) of the waveguide lying in the normal dispersion regime of our proposed design. On the other hand, due to perturbations induced by even-order dispersions terms, non solitonic radiation (NSR) with soliton fission is generated on both sides of the input spectrum that are clearly observed in Figs. 4 and 5. Since the GVD curve of this rib waveguide has two ZDWs and a strong NSR is produced in the stoke-side of the SC spectrum right after the second ZDW (located at around  $4.8 \mu\text{m}$ ) of the GVD curve which is only due to the soliton suppression effect. As the dispersion slope ( $dD/d\lambda$ ) of the GVD curve in the vicinity of the second ZDW is negative, owing to the spectral-recoil effect (soliton suppression), the negative dispersion slope has significantly modified the SC spectrum through the generation of strong redshifted dispersive wave, allowing the SC generation is extended further into the MIR regime up to  $8 \mu\text{m}$  (Fig. 4(a), 4(c), and 4(d)) and  $10 \mu\text{m}$  (Fig. 5(a), 5(c), and 5(d)) for the peak powers of  $0.5 \text{ kW}$  and  $3 \text{ kW}$ , respectively.

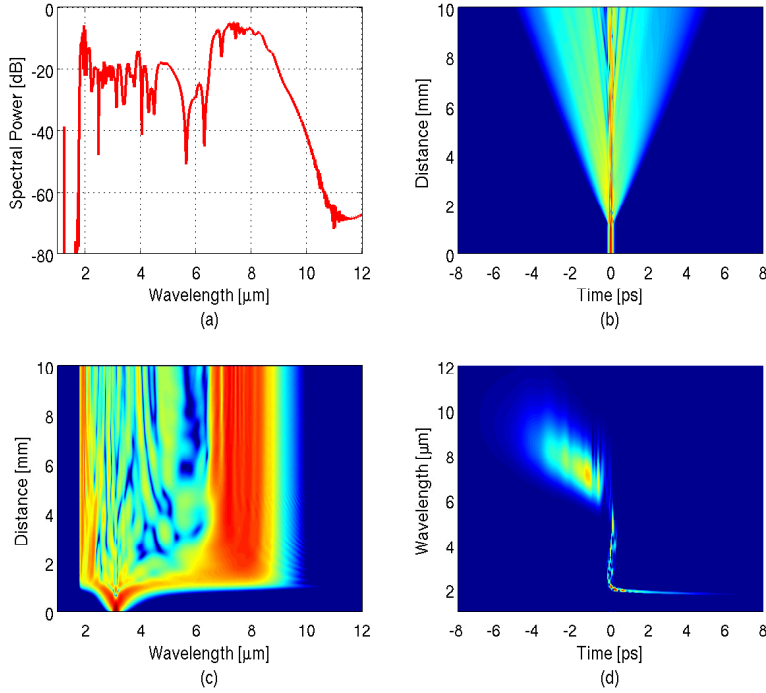


**Fig. 5** Spectral evolution along the waveguide length at a wavelength of  $3.1 \mu\text{m}$  for the peak power of 3 kW: (a) spectrum; (b) temporal density; (c) spectral density; and (d) spectrogram.

## 5 Conclusions

In conclusion, we have demonstrated that ultra-broadband MIR SC can be generated using dispersion-tailored  $\text{Ge}_{11.5}\text{As}_{24}\text{Se}_{64.5}$  chalcogenide glass air-clad rib-waveguide employing  $\text{MgF}_2$  glass as its lower cladding. Using  $\text{MgF}_2$  as a lower cladding which helps to keep the field inside the waveguide due to having high index contrast between the core-cladding interface of the waveguide. Eventually high index contrast enables the waveguide enhancing nonlinear interaction through reducing the effective mode area which effectively helps to produce ultra-broadband SC spectra at the waveguide output. Using pump pulses at a wavelength of  $3.1 \mu\text{m}$  with a relatively low peak power of 0.5 kW, we obtained a SC spectrum covering a wavelength range from  $1.8 \mu\text{m}$  to beyond  $8 \mu\text{m}$  ( $> 2$  octaves). This is the broadest MIR SC realized at a relatively low peak power of 0.5 kW using a GeAsSe-based chalcogenide planar waveguide reported so far. Our analysis also show that MIR SC can be extended over in the wavelength range  $1.8\text{-}10 \mu\text{m}$  with a moderate peak power of 3 kW.

## References

1. Aggarwal, I. D. and Sanghera, J. S.: Development and applications of chalcogenide glass optical fibers at NRL. *J. Optoelectron. Adv. Mater.* **4**(3), 665–678 (2002).
2. Andreasen, J., Bhal, A., and Kolesik, M.: Spatial effects in supercontinuum generation in waveguides. *Opt. Exp.* **22**(21), 25756–25767 (2014).
3. Bass, M., Li, G., and Stryland, E.V.: *Hand Book of Optics*. The McGraw-Hill, New York (2010).
4. Dudley, J. M., Genty, G., and Coen, S.: Supercontinuum generation in photonic crystal fiber. *Rev. Mod. Phys.* **78**, 1135–1184 (2006).
5. Dudley, J. M. and Taylor, J. R.: Ten years of nonlinear optics in photonic crystal fiber. *Nat. Photonics* **3**, 85–90 (2009).
6. Eggleton, B. J., Luther-Davies, B., and Richardson, K.: Chalcogenide photonics. *Nat. Photonics* **5**, 141–148 (2011).
7. Fatome, J., Fortier, C., Nguyen, T. N., Chartier, T., Smektala, F., Messaad, K., Kibler, B., Pitois, S., Gadret, G., Finot, C., Troles, J., Desevedavy, F., Houizot, P., Renversez, G., Brilland, L., and Traynor, N.: Linear and nonlinear characterizations of chalcogenide photonic crystal fibers. *J. Lightwave Technol.* **27**(11), 1707–1715 (2009).
8. Gai, X., Madden, S., Choi, D. Y., Bulla, D., and Luther-Davies, B.: Dispersion engineered  $\text{Ge}_{11.5}\text{As}_{24}\text{Se}_{64.5}$  nanowires with a nonlinear parameter of  $136 \text{ W}^{-1}\text{m}^{-1}$  at 1550 nm. *Opt. Exp.* **18**(18), 18866–18874 (2010).
9. Gai, X., Han, T., Prasad, A., Madden, S., Choi, D. Y., Wang, R., Bulla, D., and Luther-Davies, B.: Progress in optical waveguides fabricated from chalcogenide glasses. *Opt. Exp.* **18**(25), 26635–26646 (2010).
10. Gai, X., Choi, D., Madden, S., Yang, Z., Wang, R., and Luther-Davies, B.: Supercontinuum generation in the mid-infrared from a dispersion-engineered  $\text{As}_2\text{S}_3$  glass rib waveguide. *Opt. Lett.* **37**(18), 3870–3872 (2012).
11. Granzow, N., Stark, S. P., Schmidt, M. A., Tverjanovich, A. S., Wondraczek, L., and Russell, P. St. J.: Supercontinuum generation in chalcogenide-silica step-index fibers. *Opt. Exp.* **19**(21), 21003–21010 (2011).
12. Hu, J., Menyuk, C. R., Shaw, L. B., Sanghera, J. S., and Aggarwal, I. D.: Maximizing the bandwidth of supercontinuum generation in  $\text{As}_2\text{Se}_3$  chalcogenide fibers. *Opt. Exp.* **18**(3), 6722–6739 (2010).
13. Hudson, D. D., Baudisch, M., Werdehausen, D., Eggleton, B. J., and Biegert, J.: 1.9 octave supercontinuum generation in a  $\text{As}_2\text{S}_3$  step-index fiber driven by mid-IR OPCPA. *Opt. Lett.* **39**(19), 5752–5755 (2014).
14. Karim, M. R., Rahman, B. M. A., and Agrawal, G. P.: Dispersion engineered  $\text{Ge}_{11.5}\text{As}_{24}\text{Se}_{64.5}$  nanowire for supercontinuum generation: A parametric study. *Opt. Exp.* **22**(25), 31029–31040 (2014).
15. Karim, M. R., Rahman, B. M. A., and Agrawal, G. P.: Mid-infrared supercontinuum generation using dispersion-engineered  $\text{Ge}_{11.5}\text{As}_{24}\text{Se}_{64.5}$  chalcogenide channel waveguide. *Opt. Exp.* **23**(5), 6903–6914 (2015).
16. Kubat, I., Petersen, C. R., Moller, U. V., Seddon, A. B., Benson, T. M., Brilland, L., Mechin, D., Moselund, P. M., and Bang, O.: Thulium pumped mid-infrared 0.9–9  $\mu\text{m}$  supercontinuum generation in concatenated fluoride and chalcogenide glass fibers. *Opt. Exp.* **22**(4), 3959–3967 (2014).
17. Lamont, M. R. E., Sterke, C. M., and Eggleton, B. J.: Dispersion engineering of highly nonlinear  $\text{As}_2\text{S}_3$  waveguides for parametric gain and wavelength conversion. *Opt. Exp.* **15**(15), 9458–9463 (2007).
18. Lamont, M. R. E., Luther-Davies, B., Choi, D. Y., Madden, S., and Eggleton, B. J.: Supercontinuum generation in dispersion engineered highly nonlinear ( $\gamma = 10 \text{ /W/m}$ )  $\text{As}_2\text{S}_3$  chalcogenide planar waveguide. *Opt. Exp.* **16**(19), 14938–14944 (2008).
19. Ma, P., Choi, D. Y., Yu, Y., Gai, X., Yang, Z., Debbarma, S., Madden, S., and Luther-Davies, B.: Low-loss chalcogenide waveguides for chemical sensing in the mid-infrared. *Opt. Exp.* **21**(24), 29927–29937 (2013).
20. Møller, U., Yu, Y., Kubat, I., Petersen, C. R., Gai, G., Brilland, L., Mechin, D., Caillaud, C., Troles, J., Luther-Davies, B., and Bang, O.: Multi-milliwatt mid-infrared supercontinuum generation in a suspended core chalcogenide fiber. *Opt. Exp.* **23**(3), 3282–3291 (2015).

21. Petersen, C. R., Møller, U., Kubat, I., Zhou, B., Dupont, S., Ramsay, J., Benson, T., Sujecki, S., Abdel-Moneim, M., Tang, Z., Furniss, D., Seddon, A., and Bang, O.: Mid-infrared supercontinuum covering the 1.4-13.3  $\mu\text{m}$  molecular fingerprint region using ultra-high NA chalcogenide step-index fiber. *Nat. Photonics* **8**, 830–834 (2014).
22. Rahman, B. M. A. and Davies, J. B.: Finite-element solution of integrated optical waveguides. *J. Lightwave Technol.* **2**, 682–688 (1984).
23. Rahman, B. M. A. and Davies, J. B.: Vector- $H$  finite element solution of GaAs/GaAlAs rib waveguides. In proceedings of IEE **132**(6), 349–353 (1985).
24. Shaw, L. B., Gattass, R. R., Sanghera, J. S., and Aggarwal, I. D.: All-fiber mid-IR supercontinuum source from 1.5 to 5  $\mu\text{m}$ . *Proc. SPIE* **7914** (2011).
25. Silva, F., Austin, D. R., Thai, A., Baudisch, M., Hemmer, M., Faccio, D., Couairon, A., and Biegert, J.: Multi-octave supercontinuum generation from mid-infrared filamentation in a bulk crystal. *Nat. Commun.* **3**(807), 1–5 (2012).
26. Yu, Y., Gai, X., Wang, T., Ma, P., Wang, R., Yang, Z., Choi, D., Madden, S., and Luther-Davies, B.: Mid-infrared supercontinuum generation in chalcogenides. *Opt. Mater. Exp.* **3**(8), 1075–1086 (2013).
27. Yu, Y., Zhang, B., Gai, X., Ma, P., Choi, D., Yang, Z., Wang, R., Debbarma, S., Madden, S., and Luther-Davies, B.: A broadband, quasi-continuous, mid-infrared supercontinuum generated in a chalcogenide glass waveguide. *Laser Photonics Rev.* pp. 1–7 (2014).
28. Yu, Y., Gai, X., Zhai, C., Qi, S., Guo, W., Yang, Z., Wang, R., Choi, D., Madden, S., and Luther-Davies, B.: 1.8-10  $\mu\text{m}$  mid-infrared supercontinuum generation in a step-index chalcogenide fiber using low peak pump power. *Opt. Lett.* **40**(6), 1081–1084 (2015).
29. Weiblen, R. J., Docherty, A., Hu, J., and Menyuk, C. R.: Calculation of the expected bandwidth for a mid-infrared supercontinuum source based on  $\text{As}_2\text{S}_3$  chalcogenide photonic crystal fibers. *Opt. Exp.* **18**(25), 26666–26674 (2010).
30. Wei, C., Zhu, X., Norwood, R. A., Seng, F., and Peyghambarian, N.: Numerical investigation on high power mid-infrared supercontinuum fiber lasers pumped at 3  $\mu\text{m}$ . *Opt. Exp.* **21**(24), 29488–29504 (2013).